

Is Quantification of Bolus Tracking MRI Reliable Without Deconvolution?

Joanna E. Perthen,^{1,2*} Fernando Calamante,^{1,2} David G. Gadian,^{1,2} and Alan Connelly^{1,2}

Bolus tracking data obtained with paramagnetic intravascular tracers are commonly analyzed and quantified by the direct measurement of properties of the tissue concentration-time curve (e.g., time to peak (TTP)). The measurement of these “summary parameters” is used as an accessible alternative approach to the complex deconvolution procedure, and provides indirect measures of perfusion. However, summary parameters do not take into account differences in arterial input functions (AIFs) or residue functions ($R(t)$) between patients or studies. Simulations were performed to assess the variability of summary parameters over a realistic range of AIFs and for differing $R(t)$, to establish whether they can be used as reliable measures of tissue perfusion status. Results showed that the value of each summary parameter investigated is highly dependent upon both the AIF and $R(t)$. The referencing of summary parameters to their corresponding value in the AIF or in normal tissue is a method commonly used to normalize results, but this approach did not lead to any measures that were independent of both the AIF and $R(t)$ in this study. The results presented here show that the use of summary parameters requires considerable caution, since tissue or patient types can easily be incorrectly classified due to the effect of variations in patient AIF and $R(t)$. Magn Reson Med 47:61–67, 2002. © 2002 Wiley-Liss, Inc.

Key words: perfusion; cerebral blood flow; arterial input function; numerical simulations; deconvolution

Dynamic susceptibility contrast (DSC) MRI is increasingly used for the measurement of cerebral perfusion (1). This method requires the injection of a bolus of a paramagnetic intravascular contrast agent, and the rapid measurement of the MR signal loss caused by the passage of the bolus through the tissue. This signal loss can be converted to a concentration-time curve of contrast agent within the tissue, $C(t)$. Using principles of indicator dilution theory, $C(t)$ within a region of interest (ROI) can be expressed as a convolution (1,2):

$$C(t) = \frac{\rho}{k_H} (CBF) \cdot (C_a(t) \otimes R(t)) \quad [1]$$

where $C_a(t)$ is the arterial input function (AIF), i.e., the concentration of tracer entering the ROI, and $R(t)$ is the residue function, which describes the fraction of contrast agent remaining in the ROI at time t , following the injection of an ideal bolus at $t = 0$. CBF is cerebral blood flow, ρ is the density of brain tissue, and k_H accounts for the

difference in hematocrit between capillaries and large vessels.

There are two commonly used approaches to the analysis and quantification of DSC data. The first requires measurement of the AIF in order to perform the deconvolution of $C(t)$ using Eq. [1] (2). This method can produce direct information about the physiological parameters CBF, cerebral blood volume (CBV), and mean transit time (MTT), but involves very time-consuming postprocessing. The second approach uses summary parameters calculated directly from the profile of the $C(t)$ curve (e.g., time to peak (TTP), maximum peak concentration (MPC), etc.). This is a commonly used method (see for example Refs. 3–10) because the analysis of data is fast and straightforward, and does not necessarily require measurement of the AIF. However, summary parameters can only provide indirect measures of perfusion, although they are frequently quoted as approximations to physiological variables despite early studies indicating that this is not the case (11).

As can be seen from Eq. [1], the concentration-time curve measured within the tissue depends not only upon the CBF within that area, but also upon the particular AIF and $R(t)$ of the region. Variations in injection conditions and patient physiology will produce AIFs that differ between individuals, and $R(t)$ may also vary between patients as well as regionally within the brain—particularly in the presence of pathologic hemodynamics. The calculation of summary parameters (in contrast to the deconvolution method) takes no account of the variations in these two functions. Despite the frequent use of summary parameters in the analysis of perfusion data, as yet there has been no reported study to assess the reliability and reproducibility of these measures under conditions of varying AIF and $R(t)$.

This work presents simulations used to investigate the behavior of a number of summary parameters over a realistic range of AIFs, to ascertain whether any summary parameters can be used as reliable indicators of perfusion. The referencing of summary parameters (formation of ratios and differences) to the corresponding parameter either in the AIF or a region of normal tissue (e.g., contralateral side or cerebellum) is a common method of presenting results in an attempt at “normalization” before making comparisons between subjects or studies. The effects of such a correction method were also investigated. In addition, since the actual form of $R(t)$ in the brain is not clear, simulations were performed using two models of the residue function to assess the effects of $R(t)$ on summary parameter variability.

METHODS

The simulation of $C(t)$ requires the modeling of $C_a(t)$ and $R(t)$ in order to perform the convolution in Eq. [1]. For

¹Radiology and Physics Unit, Institute of Child Health, University College London, London, UK.

²Great Ormond Street Hospital for Children NHS Trust, London, UK.

Grant sponsor: Wellcome Trust.

*Correspondence to: Joanna Perthen, Unit of Biophysics, Institute of Child Health, University College London, 30 Guilford Street, London WC1N 1EH, UK. E-mail: jperthen@ich.ucl.ac.uk

Received 10 April 2001; revised 19 July 2001; accepted 6 August 2001.

© 2002 Wiley-Liss, Inc.
DOI 10.1002/mrm.10020

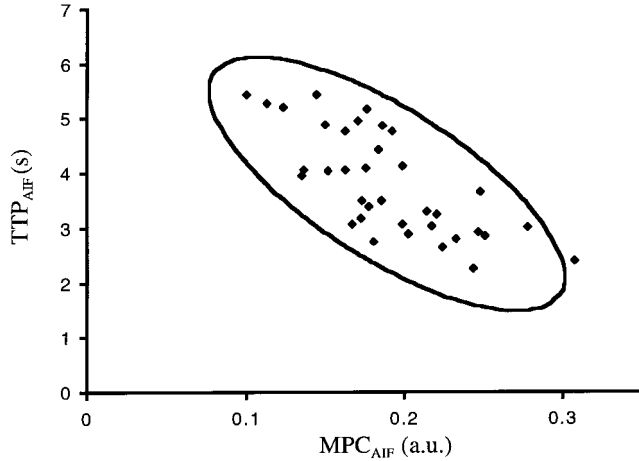


FIG. 1. TTP_{AIF} vs. MPC_{AIF} data from a sample of 36 children. The solid line indicates the 95% confidence interval for this distribution (see text for details regarding injection procedure).

simplicity, both ρ and k_H in Eq. [1] were set to 1 for the remainder of this study.

Simulations of $C_a(t)$

The AIF is commonly modeled as a gamma-variate function (12):

$$C_a(t) = C_0 t^r e^{-tb} \quad [2]$$

where parameters r and b define the shape of the rise and decay of the curve, and C_0 is a scaling factor determined by the quantity of contrast agent injected. The value of C_0 for each simulated AIF was chosen so as to normalize the volume of contrast agent injected to a constant value (i.e., $C_a(t)$ was scaled to a fixed area; in this case, $\int C_a(t) dt = 1$). Pairs of r and b values that covered a range of AIFs typically obtained in vivo were generated. An appropriate range for these two parameters was determined using actual AIF data from 36 children (0.5–17.5 years old; median 11.5 years) scanned at Great Ormond Street Hospital for Children. Patient data were acquired on a 1.5T Siemens Vision system using a spin-echo echo-planar imaging sequence (TE/TR = 0.1/1.5 s, 128×128 , 5 mm slice thickness), with a 0.1–0.15 mmol/kg body weight dose of Gd-DTPA contrast agent administered intravenously (rate 3–7 ml/s) using an MR-compatible power injector (Medrad Inc., Pittsburgh, PA). For each patient, pixels within the middle cerebral artery (MCA) were selected manually (on the contralateral side if abnormalities were present in the MCA region), and Eq. [2] was fitted to the average concentration-time curve for these pixels to produce the AIF. Rather than characterizing each AIF by its r and b (which have no direct physical meaning), the AIFs were characterized by their TTP_{AIF} ($TTP_{AIF} = r/b$) and MPC ($MPC_{AIF} = (r/b)^r e^{-r} C_0$); note that C_0 is a function of r and b because the area was scaled to a fixed value (see above)). This allows a simpler interpretation of the AIF range. The resulting distribution of patient TTP_{AIF} and MPC_{AIF} is shown in Fig. 1. The two AIF parameters cover broad ranges but are clearly

correlated, indicating that the values of the parameters in Eq. [2] cannot vary freely. The AIF distribution was characterized by its mean and 95% confidence interval ellipsoid; see Fig. 1. The mean values of TTP_{AIF} and MPC_{AIF} were 3.80 s and 0.19, respectively (corresponding to $r = 3.44$ and $b = 0.91 \text{ s}^{-1}$). The 95% confidence interval ellipsoid shows TTP_{AIF} ranging from 1.5–6.1 s and MPC_{AIF} from 0.08–0.30 (arbitrary units). This range was evenly sampled by drawing a grid aligned with the ellipsoid, and using the resulting grid points (pairs of TTP_{AIF} and MPC_{AIF} , $N = 23$) to generate the set of simulated AIFs from their corresponding r and b values.

DSC data obtained for a small group of adult patients (18–37 years old, $N = 11$) at our institution indicates that a similarly wide range of AIFs is also observed within the adult population, characterized by a longer mean TTP_{AIF} and lower mean MPC_{AIF} than the child data presented in Fig. 1. However, more data are required to reliably determine the AIF range for adults, and therefore the simulations reported in this study are based on the range of AIFs observed in the data from children.

Simulations of $R(t)$

The actual form of $R(t)$ in vivo remains unknown, and since it depends upon the local vascular structure, it is possible that $R(t)$ may vary between subjects, or even within a subject. For these reasons, simulations were performed using two common models to describe this function. First, an exponential function was used, based on a model of the vascular bed as one single, well-mixed compartment (13,14):

$$R(t) = e^{-t/MTT}. \quad [3]$$

Second, a box function was used to simulate plug flow within the vasculature (2):

$$\begin{aligned} R(t) &= 1 & (t \leq MTT) \\ R(t) &= 0 & (t > MTT). \end{aligned} \quad [4]$$

CBF and MTT Values

In order to simulate $C(t)$ using Eq. [1], values of CBF and MTT are also required. These two parameters are linked by the central volume theorem: $CBF = CBV/MTT$ (15,16). Typical literature values corresponding to normal gray and white matter in humans were used (1,17–20):

- Gray matter: CBF = 60 ml/100 g/min; MTT = 4 s; CBV = 4 ml/100 g
- White matter: CBF = 22 ml/100 g/min; MTT = 5.5 s; CBV = 2 ml/100 g.

Simulations were also performed for the case of abnormal (ischemic) gray matter. A CBF of 20 ml/100 g/min was chosen as representative of such tissue, since it has been suggested that cellular dysfunction occurs at around this value (21). However, the choice of MTT and CBV at this flow value is not straightforward because there is little agreement within the literature on the behavior of these parameters under conditions of decreasing CBF (22–27). For the purposes of the present simulations, we chose to

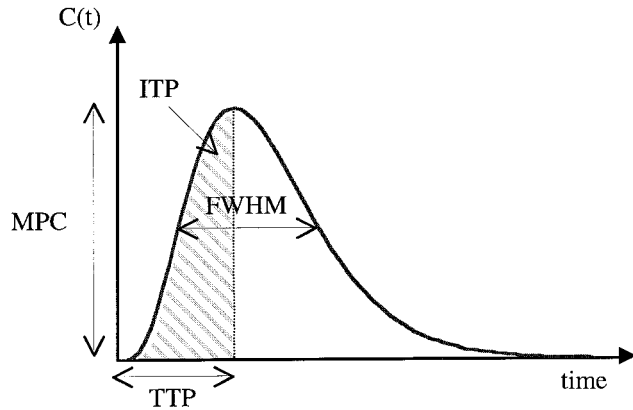


FIG. 2. Schematic tissue concentration-time curve illustrating summary parameters (see text for definitions).

use the following values for abnormal gray matter: CBF = 20 ml/100 g/min; MTT = 9.9 s; CBV = 3.3 ml/100 g.

Summary Parameters Measured

The convolution (Eq. [1]) was evaluated for each tissue type considered, using both the exponential and the box residue functions with each of the simulated AIFs, i.e., a total of 138 $C(t)$ curves were simulated. For each of the resulting simulated concentration-time curves, the more commonly used summary parameters (see Fig. 2) were calculated: 1) MPC; 2) TTP; 3) full width at half maximum (FWHM); 4) integral to peak, $ITP = \frac{\int_0^{TTP} C(t) dt}{\int_0^{TTP} C_a(t) dt}$; 5) normalized first moment, “MTT” = $\frac{\int tC(t) dt}{\int C(t) dt}$, referred to as “MTT” since this measure is commonly used as a quantitative approximation to MTT; and 6) a perfusion index, “CBF” = $\frac{CBV}{“MTT”}$, where $CBV = \frac{\int C(t) dt}{\int C_a(t) dt}$, i.e., the normalized total area under the peak.

It should be noted that the parameter CBV (as calculated above) is fixed for a constant CBF and MTT ($CBV = CBF \times MTT$), and is also measured in this way in the deconvolution methods. CBV depends only on the area beneath the curves and not on their shape, and so is not affected by variability in patient AIF or $R(t)$. In real data, errors in the measurement of CBV only result from inaccurate specifi-

cation of the concentration-time curves due to noise, poor fitting of data, or contribution from recirculation. Although CBV is a useful and often used parameter, it is not considered as one of the “summary parameters” investigated in this study due to the lack of any source of error in simulated data.

To investigate the dependency of the summary parameters on the different AIFs, 3D and contour plots were created for each parameter as a function of MPC_{AIF} and TTP_{AIF} . A flat 3D plot would imply that the parameter is independent of the AIF, which is one of the requirements for a meaningful measure.

Two methods commonly used in the analysis of summary parameters were investigated to assess whether these approaches minimized any AIF dependency found. The first involved calculating ratios or differences between each summary parameter and the corresponding value in the AIF (e.g., $TTP - TTP_{AIF}$). The second used normal gray matter values as a reference for the ischemic tissue in a similar manner (for instance, calculation of $TTP_{abnormal} - TTP_{normal}$, $MPC_{abnormal}/MPC_{normal}$ etc.) since many studies use contralateral or cerebellum values in this way.

RESULTS

Dependency on AIF

The simulated AIFs produced a range of $C(t)$ curves with very different profiles. Results from the simulations showed that for a given $R(t)$, CBF, CBV, and MTT, every parameter measured in $C(t)$ varied considerably over the AIF range (see Table 1). Figure 3 shows one example of a 3D plot of a summary parameter (TTP). It can be seen that the surface slopes considerably, with TTP varying between 3.9 and 9.5 s for the range of AIF values used.

Most parameters showed a “smooth,” or planar variation over the AIF range similar to that shown in Fig. 3. The most extreme exception to this trend was FWHM, when calculated for abnormal gray matter with a box $R(t)$. The 3D plot for this parameter is shown in Fig. 4, where it can be seen that the majority of the variation in FWHM values is seen in one portion of the 95% AIF confidence ellipsoid.

Dependency on $R(t)$

ITP showed the smallest percentage variations over the AIF range, but showed high dependency on the assumed

Table 1
Range Shown by Each Summary Parameter Over the Range of Simulated AIFs

Tissue type	Gray matter CBF = 60 ml/100 g/min MTT = 4 s CBV = 4 ml/100 g		White matter CBF = 22 ml/100 g/min MTT = 5.5 s CBV = 2 ml/100 g		Abnormal gray matter CBF = 20 ml/100 g/min MTT = 9.9 s CBV = 3.3 ml/100 g	
	Exponential	Box	Exponential	Box	Exponential	Box
MPC ($\times 10^{-3}$; arbitrary units)	3.0–5.3	3.9–8.3	1.3–2.2	1.9–3.4	1.6–2.4	2.6–3.3
TTP (s)	3.9–9.5	4.3–8.3	4.3–10.2	5.6–9.3	5.0–11.6	9.9–12.4
FWHM (s)	6.5–12.4	4.6–9.2	7.7–13.9	5.7–9.6	11.0–17.9	9.9–11.8
ITP ($\times 10^{-3}$)	11.5–14.3	13.2–19.0	5.3–6.9	7.1–11.1	6.8–9.9	14.6–23.9
“MTT” (s)	6.7–12.3	4.7–10.3	8.2–13.8	5.5–11.0	12.6–18.2	7.7–13.2
“CBF” (ml/100 g/min)	19.6–35.6	23.4–50.6	8.8–14.7	11.0–22.0	10.9–15.7	15.0–25.7

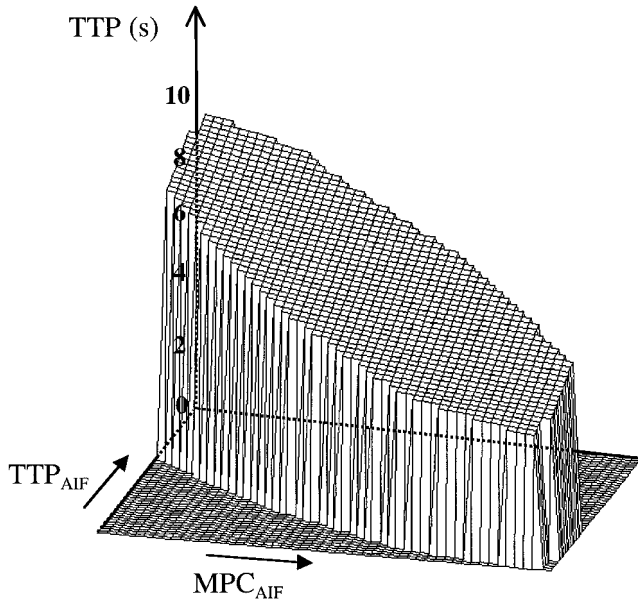


FIG. 3. 3D plot of tissue TTP as a function of MPC_{AIF} and TTP_{AIF} for normal gray matter and exponential residue function; only TTP values calculated within the AIF 95% confidence ellipsoid (see Fig. 1) are shown. TTP covers a wide range, with values varying between 3.9 and 9.5 s.

model for $R(t)$. The contour plots in Fig. 5 highlight the differences in range and slope seen on 3D plots of ITP for the two residue functions.

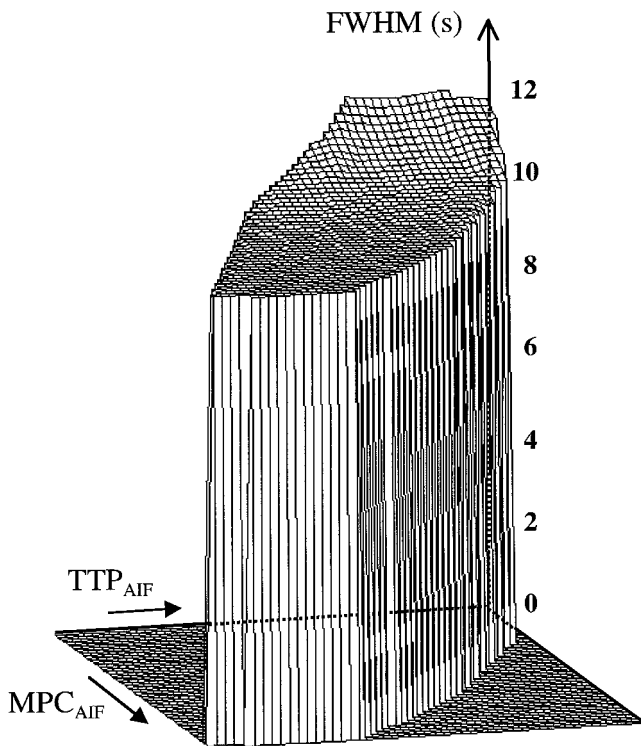
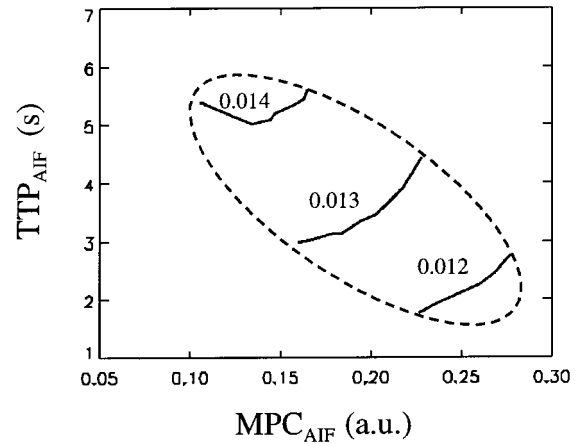
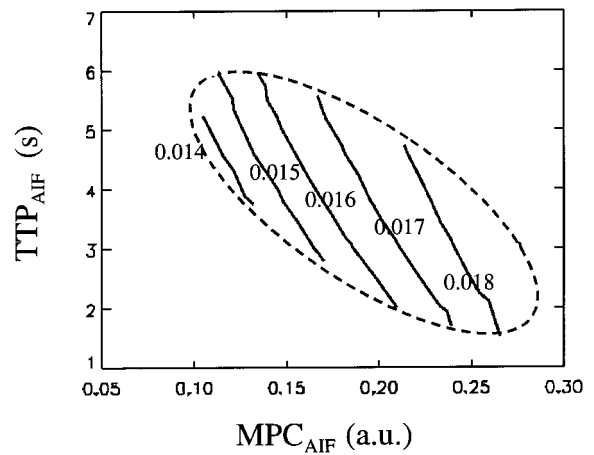


FIG. 4. 3D plot of tissue FWHM as a function of MPC_{AIF} and TTP_{AIF} for abnormal gray matter and box $R(t)$; only FWHM values calculated within the AIF 95% confidence ellipsoid (see Fig. 1) are shown. This parameter is unusual in that the variation seen is predominantly in one portion of the AIF confidence ellipsoid.



a



b

FIG. 5. Plots showing contours of ITP as a function of MPC_{AIF} and TTP_{AIF} for normal gray matter, using (a) an exponential and (b) a box residue function. Each contour (solid line) is labeled with its ITP value. The AIF 95% confidence interval ellipsoid (see Fig. 1) is shown in each case by the dotted line. The angle and range of the ITP contours are very different for the two residue functions, in contrast to the other parameters investigated.

For each of the other parameters, the contour plots showed contour lines that were similarly angled for each of the two residue functions, indicating a similar direction of slope over the AIF range in each case. However, quantitative values for MPC and “CBF” were generally slightly higher using the box function than the exponential for a particular AIF (see Table 1). This trend was reversed for the timing parameters, TTP, FWHM, and “MTT,” which produced generally lower values with the box function.

Gray and White Matter

The behavior described above was qualitatively very similar for both gray and white matter. The timing parameters (TTP, FWHM, and “MTT”) were also quantitatively similar for both tissue types, but MPC and “CBF” values were much lower for white matter. ITP was again the anomaly, showing a different range and pattern of contour lines for the two tissue types.

Relative Summary Parameters

Referencing each summary parameter to the corresponding parameter in the AIF did not remove the AIF depen-

dency, with the exception of “MTT.” In this case, the value of “MTT” – “MTT”_{AIF} was found to be constant over the AIF range, but its value was dependent upon $R(t)$, such that:

$$\text{Exponential } R(t): \text{“MTT”} - \text{“MTT”}_{AIF} = MTT \quad [5]$$

$$\text{Box } R(t): \text{“MTT”} - \text{“MTT”}_{AIF} = \frac{MTT}{2}. \quad [6]$$

All other parameters retained significant dependency on the AIF when referenced to the corresponding parameter in this function. In the case of FWHM, the value of $FWHM - FWHM_{AIF}$ was relatively stable using the exponential $R(t)$ (varying between 3 and 3.8 s in the gray matter case compared to the original range of 6.5–12.4 s for FWHM alone), but has a high dependency on $R(t)$ (ranging from 0.3–1.3 s for the box function). $TTP - TTP_{AIF}$ was a more promising measure, with extremes of 2 and 3.6 s for an exponential $R(t)$, and 2.2 and 2.8 s for a box—a considerable improvement (narrower time interval) on the wide range shown in Fig. 3.

In the case of referencing each summary parameter measured in abnormal gray matter to the corresponding summary parameter for normal gray matter (assuming the same AIF and form of $R(t)$ for each), the resulting ratios and differences again showed a substantial dependency on the particular AIF. Once more, the exception was “MTT,” where, in the case of an exponential $R(t)$:

$$\text{“MTT”}_{abnormal} - \text{“MTT”}_{normal} = MTT_{abnormal} - MTT_{normal} \quad [7]$$

which follows from Eq. [5]. However, as before, the value of “MTT”_{abnormal} – “MTT”_{normal} depends upon the residue function used. The AIF dependency could in some other cases be reduced, e.g., $TTP_{abnormal} - TTP_{normal}$ covers a much smaller range (≈ 1.5 s between AIF extremes) than $TTP_{abnormal}$ (≈ 6 s) and is therefore a more reliable measure (Fig. 6). Similarly, forming ratios for TTP, MPC, “MTT,” and FWHM, or calculating $FWHM_{abnormal} - FWHM_{normal}$ produced significantly more stable measures than their actual values in each case.

DISCUSSION

The use of summary parameters as measures of cerebral perfusion is still common practice, despite early criticism (11). This is because the deconvolution method, which is generally regarded as a reliable method of producing meaningful CBF, CBV, and MTT values, requires time-consuming data processing. The results presented here support concerns over summary parameters, and have further implications regarding their use. The simulations reveal that summary parameters of the concentration-time curve measured within the tissue are highly dependent on the patient’s AIF for both residue functions tested, and also provide an estimate of the potential magnitude of the errors introduced. Following the injection of a bolus of contrast agent, the shape of the resulting AIF can vary dramatically between subjects (see Fig. 1), presumably due

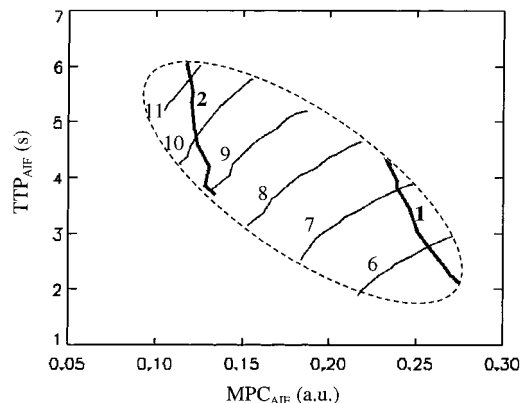


FIG. 6. Plot showing contours of $TTP_{abnormal}$ (thin lines) and $TTP_{abnormal} - TTP_{normal}$ (thick lines) for normal gray matter using an exponential residue function. Contours are labeled in seconds. The dotted line shows the AIF 95% confidence interval ellipsoid (see Fig. 1). $TTP_{abnormal} - TTP_{normal}$ covers a much narrower time interval than $TTP_{abnormal}$.

to the influence of patient physiology (cardiac output, vascular structure, etc.) and injection conditions (cannula size, injection rate, etc.). $R(t)$ may also vary between individuals, as well as spatially throughout the brain, further complicating results. Therefore, the use of summary parameters as a measure of tissue perfusion status is potentially misleading.

The same trends were observed in simulations performed for both gray and white matter. The quantitative differences between summary parameter values in the two tissue types can be explained by the form of Eq. [1] and the residue functions used. Gray and white matter have very different CBF values, which affects the scaling of the $C(t)$ curve, leading to lower MPC and “CBF” values in the white matter. However, the MTT values for each tissue type are similar, leading to comparable timing parameter values for the two tissue types.

Summary parameters are commonly used as approximations to physiological parameters; for instance, FWHM and “MTT” are used as quantitative measures of MTT, and similarly MPC and “CBF” are used as CBF. Our simulations demonstrate that this practice can create a misleading picture. For instance, given an actual MTT value of 4 s, the calculated “MTT” for gray matter was shown to vary between 4.7 and 12.3 s. Correspondingly, if “CBF” is then calculated using the central volume theorem, results varying between 20 and 50 ml/100 g/min are obtained for an actual CBF of 60 ml/100 g/min (see Table 1). “MTT” and “CBF” are biased estimators of their true values, with “MTT” substantially overestimating its actual value in almost every case, and “CBF” underestimating the true CBF. Summary parameters are also often used as indirect measures of tissue perfusion in their own right (e.g., TTP), to reflect some aspect of the hemodynamic status of the tissue. In either case, any comparison of results between patients is unreliable since differences in patient AIF can produce dramatically different summary parameter values under conditions of identical CBF, CBV, and MTT. It is important to note that these large errors associated with any summary parameter measurement remain regardless

of the precision with which the actual measurement is made, since their source is the differences in patient AIF.

In an attempt to “normalize” results before making comparisons between subjects, summary parameters are often reported as ratios or differences between abnormal and normal values. The simulations performed in this work showed that this technique does not remove AIF dependency, with the exception of “MTT,” for which a measure independent of the AIF could be created by subtraction ($“MTT”_{abnormal} - “MTT”_{normal}$). However, the AIF independence of this measure is unlikely to be useful in practice due to its demonstrated continuing dependency on the residue function. Nevertheless, in several cases, forming ratios or differences did reduce AIF dependency and led to a more reliable measure that varied over a smaller range (for example, see Fig. 6).

The referencing of each summary parameter to its AIF value (again by forming ratios and differences) was also investigated as a means of eliminating AIF dependency. Once again, this was only successful in the case of “MTT,” where it was found that $“MTT” - “MTT”_{AIF}$ is AIF independent, but that its value depends on $R(t)$. This is consistent with findings reported by Axel (28). For all other summary parameters, AIF dependency remained but was in some cases reduced, i.e., a more suitable parameter than the actual value could be found (e.g., $TTP - TTP_{AIF}$ rather than TTP). This allows an improvement in the objective determination of the perfusion status, but these values must still be interpreted with caution since any differences between subjects cannot be attributed solely to hemodynamic differences, due to the remaining dependency on the AIF.

The present simulations have shown that the referencing of summary parameters does not in general eliminate the differences caused by variations in AIF, even in the “ideal” case presented here, in which $R(t)$ and $C_a(t)$ are uniform across the brain, and summary parameters can be measured perfectly accurately. These differences remain because the effects causing spreading of the bolus are not generally additive, since $C(t)$ is described by a convolution. It can be expected that the variability found in summary parameter values might be even greater in real data, where $C_a(t)$ (and potentially $R(t)$) may vary across the brain, and summary parameters cannot be measured perfectly accurately.

Many studies use summary parameters to determine thresholds that are used to segregate tissue into regions depending on their physiological status (e.g., core and penumbra in the case of stroke patients). Results are commonly used to predict how tissue status will develop. The present simulations show that tissue can easily be classified incorrectly due to summary parameter variability. For instance, the measure $TTP_{abnormal} - TTP_{normal}$ in gray matter can vary between 0.9 and 2.4 s over the AIF range studied (for a fixed $CBF_{normal} = 60$ ml/100 g/min and $CBF_{abnormal} = 20$ ml/100 g/min, exponential $R(t)$). This implies that segregation of tissue regions into narrow bands based upon $TTP_{abnormal} - TTP_{normal}$ values could lead to considerable inconsistency between patients, potentially leading to the incorrect classification of tissue type and patient groups. The use of wide bands for segregation of tissue regions can reduce errors, but leads to less

detailed results. Clearly, the method of setting thresholds as a means of selecting patients suitable for a specific therapeutic intervention must be undertaken with care, since in some cases the variability due to AIF differences could be larger than the expected variation between different tissue or patient types.

The results presented in this study are based on an AIF range characteristic of children. However, our preliminary findings suggest that the implications regarding the use of summary parameters highlighted in this work also apply in the case of adults (see the Methods section). It should also be noted that the CBF, CBV, and MTT values chosen to reflect normal gray and white matter for use in the simulations were those corresponding to adult rather than child data. This is because normal values of CBF, CBV, and MTT in children have not been adequately characterized since the majority of studies measuring these parameters in normal subjects have been carried out on adults. However, the general findings of these simulations (considerable variability in summary parameter values over the AIF range) are expected to be valid regardless of the specific perfusion values, since the results for gray and white matter were very similar.

In conclusion, this study has shown that the use of summary parameters as measures of perfusion should be undertaken with caution. Ideally, parameters that are independent of patient AIF and $R(t)$ are required, but this was not the case for any of those tested in these simulations. Nevertheless, summary parameters can be effective in the identification of abnormal regions, and the most appropriate (smallest dynamic range) to use in a given study will depend on the particular application and conditions. However, summary parameter variability means that their use in defining thresholds, making within-subject comparisons, or comparing results between subjects and in follow-up studies, can potentially lead to the incorrect classification of patients with respect to their hemodynamic status, which can, in turn, influence decisions about future treatment. Deconvolution methods can, in principle, circumvent these limitations, and their use has been corroborated by recent studies (26,29–31), although full validation under varied pathological conditions is still required (32,33).

ACKNOWLEDGMENTS

We thank Dr. Martin D. King for helpful discussions. Research at the Institute of Child Health and Great Ormond Street Hospital for Children NHS Trust benefits from R&D funding received from the NHS Executive.

REFERENCES

1. Calamante F, Thomas DL, Pell GS, Wiersma J, Turner R. Measuring cerebral blood flow using magnetic resonance techniques. *J Cereb Blood Flow Metab* 1999;19:701–735.
2. Østergaard L, Weisskoff RM, Chesler DA, Gyldensted C, Rosen BR. High resolution measurement of cerebral blood flow using intravascular tracer bolus passages. Part I. Mathematical approach and statistical analysis. *Magn Reson Med* 1996;36:715–725.
3. Maeda M, Yuh WTC, Ueda T, Maley JE, Crosby DL, Zhu M-W, Magnotta VA. Severe occlusive carotid artery disease: hemodynamic assessment by MR perfusion imaging in symptomatic patients. *AJNR Am J Neuroradiol* 1999;20:43–51.

4. Nighoghossian N, Berthezene Y, Philippon B, Adeleine P, Froment JC, Trouillas P. Hemodynamic parameter assessment with dynamic susceptibility contrast magnetic resonance imaging in unilateral symptomatic internal carotid artery occlusion. *Stroke* 1996;27:474–479.
5. Neumann-Haefelin T, Wittsack H-J, Wenserski F, Siebler M, Seitz RJ, Mödler U, Freund H-J. Diffusion- and perfusion-weighted MRI. The DWI/PWI mismatch region in acute stroke. *Stroke* 1999;30:1591–1597.
6. Kluytmans M, van der Grond J, Folkers PJM, Mali WPTM, Viergever MA. Differentiation of gray matter and white matter perfusion in patients with unilateral internal carotid artery occlusion. *J Magn Reson Imaging* 1998;8:767–774.
7. Ernst T, Chang L, Itti L, Speck O. Correlation of regional cerebral blood flow from perfusion MRI and SPECT in normal subjects. *Magn Reson Imaging* 1999;17:349–354.
8. Kim JH, Lee SJ, Shin T, Kang KH, Choi PY, Kim JH, Gong JC, Choi N-C, Lim BH. Correlative assessment of hemodynamic parameters obtained with T2*-weighted perfusion MR imaging and SPECT in symptomatic carotid artery occlusion. *Am J Neuroradiol* 2000;21:1450–1456.
9. Nasel C, Azizi A, Veintimilla A, Mallek R, Schindler E. A standardized method of generating time-to-peak perfusion maps in dynamic-susceptibility contrast-enhanced MR imaging. *Am J Neuroradiol* 2000;21:1195–1198.
10. Schlaug G, Benfield A, Baird AE, Siewart B, Lövsblad KO, Parker RA, Edelman RR, Warach S. The ischemic penumbra operationally defined with diffusion and perfusion MRI. *Neurology* 1999;53:1528–1537.
11. Weisskoff RM, Chesler D, Boxerman JL, Rosen BR. Pitfalls in MR measurement of tissue blood flow with intravascular tracers: which mean transit-time? *Magn Reson Med* 1993;29:553–559.
12. Starmer CF, Clark DO. Computer computations of cardiac output using the gamma function. *J Appl Physiol* 1970;28:219–220.
13. Bassingthwaite JB, Goresky GA. In: Renkin EM, Michel CG, editors. *Handbook of physiology, section 2: the cardiovascular system*. Bethesda: American Physiology Society; 1984. p 549–626.
14. Lassen NA, Henriksen O, Sejrsen P. In: Shepherd JT, Abboud FM, editors. *Handbook of physiology, section 2: the cardiovascular system*. Bethesda: American Physiology Society; 1984. p 21–64.
15. Stewart GN. Researches on the circulation time in organs and on the influences which affect it. Parts I–III. *J Physiol (Lond)* 1894;15:1.
16. Meier P, Zierler KL. On the theory of the indicator-dilution method for measurement of blood flow and volume. *Appl Physiol* 1954;6:731–744.
17. Schreiber WG, Gückel F, Stritzke P, Schmiedek P, Schwartz A, Brix G. Cerebral blood flow and cerebrovascular reserve capacity: estimation by dynamic magnetic resonance imaging. *J Cereb Blood Flow Metab* 1998;18:1143–1156.
18. Rempp KA, Brix G, Wenz F, Becker CR, Guckel F, Lorenz WJ. Quantification of regional cerebral blood flow and volume with dynamic susceptibility contrast-enhanced MR imaging. *Radiology* 1994;193:637–641.
19. Koshimoto Y, Yamada H, Kimura H, Maeda M, Tsuchida C, Kawamura Y, Ishii Y. Quantitative analysis of cerebral microvascular hemodynamics with T2-weighted dynamic MR imaging. *J Magn Reson Imaging* 1999;9:462–467.
20. Smith AM, Grandin CB, Duprez T, Mataigne F, Cosnatd G. Whole brain quantitative CBF, CBV and MTT measurements using MRI bolus tracking: implementation and application to data acquired from hyperacute stroke patients. *J Magn Reson Imaging* 2000;12:400–410.
21. Baird AE, Warach S. Magnetic resonance imaging of acute stroke. *J Cereb Blood Flow Metab* 1998;18:583–609.
22. McKinstry RC. Practical application of perfusion imaging in adults. In: *Advanced Imaging Symposium Syllabus*, American Society of Neuro-radiology 38th Annual Meeting, Atlanta, GA, 2000. p 109–113.
23. Grubb RL, Raichle ME, Eichling JO, Ter-Pogossian MM. The effects of changes in PaCO₂ on cerebral blood volume, blood flow, and vascular mean transit time. *Stroke* 1974;5:630–639.
24. Schumann P, Touzani O, Young AR, Baron J-C, Morello R, MacKenzie ET. Evaluation of the ratio of cerebral blood flow to cerebral blood volume as an index of local cerebral perfusion pressure. *Brain* 1998;121:1369–1379.
25. Powers WJ. Cerebral hemodynamics in ischemic cerebrovascular disease. *Ann Neurol* 1991;29:231–240.
26. Sakoh M, Røhl L, Gyldensted C, Gjedde A, Østergaard L. Cerebral blood flow and blood volume measured by magnetic resonance imaging bolus tracking after acute stroke in pigs: comparison with [¹⁵O]H₂O positron emission tomography. *Stroke* 2000;31:1958–1964.
27. Zaharachuk G, Mandeville JB, Bogdanov AA, Weissleder R, Rosen BR, Marota JJA. Cerebrovascular dynamics of autoregulation and hypoperfusion: an MR study of CBF and changes in total and microvascular cerebral blood volume during hemorrhagic hypotension. *Stroke* 1999;30:2197–2205.
28. Axel L. Methods using blood pool tracers. In: Le Bihan D, editor. *Diffusion and perfusion magnetic resonance imaging*. New York: Raven Press; 1995. p 205–211.
29. Østergaard L, Johannsen P, Poulsen PH, Vestergaard-Poulsen P, Asboe H, Gee AD, Hansen SB, Cold GE, Gjedde A, Gyldensted C. Cerebral blood flow measurements by magnetic resonance imaging bolus tracking: comparison with [O-15] H₂O positron emission tomography in humans. *J Cereb Blood Flow Metab* 1998;18:935–940.
30. Østergaard L, Smith DF, Vestergaard-Poulsen P, Hansen SB, Gee AD, Gjedde A, Gyldensted C. Absolute cerebral blood flow and blood volume measured by magnetic resonance imaging bolus tracking: comparison with positron emission tomography values. *J Cereb Blood Flow Metab* 1998;18:425–432.
31. Wirestam R, Ryding E, Lindgren A, Geijer B, Holtås S, Ståhlberg F. Absolute cerebral blood flow measured by dynamic susceptibility contrast MRI: a direct comparison with Xe-133 SPECT. *MAGMA* 2000;11:96–103.
32. Calamante F, Gadian DG, Connelly A. Delay and dispersion effects in dynamic susceptibility contrast MRI: simulations using singular value decomposition. *Magn Reson Med* 2000;44:466–473.
33. Østergaard L, Chesler DA, Weisskoff RM, Sorensen AG, Rosen BR. Modeling cerebral blood flow and flow heterogeneity from magnetic resonance residue data. *J Cereb Blood Flow Metab* 1999;19:690–699.